Impact of Precursor Exposure in Spatial Atomic Layer Deposition on Process Efficiency and Film Properties

Nguyen Viet Huong, Sekkat Abderrahime, Carmen Jiménez, Delfina Munoz, Daniel Bellet, David Munoz-Rojas

Impact of Precursor Exposure in Spatial Atomic Layer Deposition on Process Efficiency and Film Properties

Viet Huong Nguyen,[1,] Abderrahime Sekkat,[2] Carmen Jiménez,[2] Delfina Muñoz,[3] Daniel Bellet,[2] David Muñoz-Rojas[2,*]*

[1] Faculty of Electrical and Electronic Engineering, Phenikaa University, Hanoi 12116, Vietnam

[2] Univ. Grenoble Alpes, CNRS, Grenoble INP, LMGP, Grenoble, France

[3] Univ. Grenoble Alpes, CEA, LITEN, INES, F-73375, Le Bourget-du-Lac, France

Abstract

Being able to control the exposure of precursors to the substrate surface is essential towards an optimum Atomic Layer Deposition (ALD) process. Conventional ALD usually requires large excesses of precursors and expensive vacuum chamber in which the precursor exposure can be controlled via the injection pulse duration followed by a delay time. A version of ALD, namely Spatial ALD (SALD), which has the same unique assets as conventional ALD but being faster, vacuum-free, and easier to scale up, has recently attracted much attention. In SALD, precursors are continuously exposed to a moving surface, and thus it is more complicated to tune precursor exposure than with conventional ALD. Here, we present a study on how to control this critical parameter in for the deposition of ZnO films using a close-proximity, open-air SALD. Our results are based on both simulations and experiments. A simple physical model supported by Comsol Multiphysics simulations has been developed to study the effect of the substrate velocity as well as the precursor concentration in the carrier gas on film growth rate. We found that the precursor entrainment by the moving substrate induces an asymmetric precursor concentration profile that affects the obtained GPC. Also, we show that the mass density and structural properties of the deposited films depend closely on the film growth rate. For instance, fast growth does not always produce dense films. Indeed, a compromise between the growth rate and the precursor consumption

should be considered to obtain both good process efficiency and high-quality films. Our findings are particularly relevant for using SALD in large-scale coating applications, in which high deposition rate and good coating density should be obtained with a minimal ALD precursor consumption.

Keywords: spatial ALD, atmospheric pressure, precursor exposure, process efficiency, substrate velocity

1. Introduction

Atomic layer deposition (ALD) has been considered as one of the best thin-film growth technologies thanks to its capability of depositing pinhole-free, conformal films at relatively low temperatures.[1–3] Over the past decades, research advances have expanded the use of this surface-controlled layer-by-layer technology beyond microelectronic applications[4,5], including the development of biosensors,[6] materials for barrier coatings[7–11] or energy conversion and storage.[12–18] However, one of the main drawbacks of ALD is a slow growth rate, which can be attributed to slow purging steps alternatively performed between different precursor injections.[19] Additionally, the use of a vacuum chamber makes conventional ALD technology more difficult and expensive to scale up towards an industrial level. In this context, a variation of ALD technique, namely spatial ALD (SALD), has been recently attracting much attention since this ALD-based technology can be applied to deposit materials at atmospheric pressure and low temperatures. Additionally, SALD provides very fast deposition rate and in a scalable fashion, while keeping the unique assets of ALD technology.[20–23] For instance, SALD is compatible with roll-to-roll technology for fast industrial thin film deposition.[24] The key point of an ALD technology is the possibility of thoroughly controlling the half-reactions between precursors and the substrate surface, and at the same time to minimize the precursor use and optimize the ALD growth rate (expressed in the thickness of the layer deposited on the surface after each ALD cycle, i.e. nm/cycle).[3,25] In an ideal ALD process, a complete monolayer of precursor molecules would be formed on the substrate surface after each precursor exposure to the substrate surface. In such an adsorption process, the amount of precursor being exposed to the surface (calculated as the product of the precursor exposure time and the precursor concentration) should be appropriately selected to achieve the saturation state of the precursor-substrate surface reaction. The determination of a

critical value of the exposure corresponding to such a complete ALD half-reaction is thus necessary. Indeed, since ALD is a self-limiting process, for a given precursor concentration in the gas phase, an exposure time longer than the critical value is not useful but causes a waste of ALD precursors, which are commonly expensive. In conventional ALD, the exposure time usually depends on the chamber/sample size, the concentration of the precursors in the gas phase, the chamber pressure, as well as the substrate temperature.

Contrarily to conventional ALD, in SALD the precursors are continuously injected onto the substrate, for instance from different gas outlets of an injection head. These reactive precursor regions are spatially separated from mixing thanks to inert gas barriers, which are alternatively located between the precursor regions. Given the close distance needed between the injection head and the substrate (~ 200 µm) to avoid precursor cross-talk, this kind of approach is commonly called close-proximity SALD.[26,27] When performing SALD with a moving substrate, the distribution of precursors to the substrate surface will be considerably affected. As a result, controlling the precursor exposure is much more complicated in the case of SALD than in ALD since there is no longer a deposition chamber, the purging step is indeed substituted by passing the substrate through an inert gas region. Obviously, the optimization of the exposure is more critical for metal precursors than for oxidizing agents, especially for large-scale applications since the ALD precursors are usually very expensive. In literature, several approaches related to modeling the ALD deposition reaction, such as adsorption kinetics or surface reaction mechanisms have been proposed.[28–31] In the case of SALD, Poodt *et al.* developed a physical model to study the deposition kinetics of Al_2O_3 when using a rotating SALD injection system,[32] in which the exposure time of precursors is simply supposed to be inversely proportional to the rotation frequency. Also, while Deng *et al.* proposed a model to quantitatively link the film growth throughput and precursor utilization, it is only based on the gas flows and precursor concentration, and other parameter such as the injector-

substrate gap or the gas entrainment due to the moving substrate are not taken into account.[33] Finally, the effect of the deposition parameters on the film properties is not discussed in previous works. Thus, in-depth studies to link the optimization of the film growth rate with ALD precursor consumption, taking into account precursor concentration, gas flow values, substrate velocity and deposition gap, and discuss the properties of the films obtained as a function of the parameters used are still needed.

In this work, we present simulation and experimental results related to tuning the precursor exposure to the substrate surface via the substrate velocity, precursor concentration in the carrier gas and substrate/injection head gap. The effect of these parameters on the growth rate and the physical properties of deposited ZnO thin films is thoroughly discussed. The study has been performed for the case of ZnO deposition using a close-proximity SALD approach. However, it can be easily extended to any material or other SALD approaches.

2. Experimental section

The deposition of ZnO films was performed with a home-made atmospheric pressure spatial atomic layer deposition (AP-SALD) system.[34] Diethylzinc (DEZ, $Zn(C_2H_5)_2$ from Sigma Aldrich) and water (H_2O) were used as zinc precursor and oxidizing agent, respectively, while nitrogen was used as carrying and purging gas. The substrate oscillated at a constant distance of 180 µm from the injection head. All samples were deposited on borosilicate glass substrates at a substrate temperature of 200 °C. Such experimental conditions have been previously used to deposit thin ZnO conformal layers at the top of silver nanowire networks to enhance both the thermal and electrical stability of such networks (see figure S1 in the supporting information).[35]

Several simulation results were obtained using Comsol Multiphysics via a combination of three modules: heat transfer in fluids, laminar flow, and transport of diluted species. The details

related to the simulations are described in part 4 of the Supporting Information. When studying the effect of the substrate velocity, other experimental parameters such as substrate temperature, the substrate/injection head gap, or nitrogen bubbling flows through zinc precursor and water (which are supposed to be directly related to reactant quantity carried to the injection head) were maintained constant. The thickness, density, and crystalline structure of the deposited films were investigated using an FS-1™ Multi-Wavelength Ellipsometer from Film Sense, an X-ray Reflectometry system (D500 Siemens), and an X-ray Diffractometry system (D8 Advance Bruker). The texture coefficients of the different ZnO films were calculated from the diffraction peak intensities relative to each other and to the standard powder pattern (ICSD 29272), as follows:

$$TC(hkl) = \frac{I(hkl)/I_0(hkl)}{\frac{1}{N}\sum I(hkl)/I_0(hkl)} \quad \text{Eq (1)}$$

where $TC(hkl)$ and $I(hkl)$ are the texture coefficient and the peak intensity of the *(hkl)* reflection peak, respectively. $I_0(hkl)$ is the *(hkl)* peak intensity in the powder pattern (considered from ICSD 29272) and *N* is the number of reflections present in the powder pattern (*N*=4 in our case). For a randomly oriented polycrystalline sample, the texture coefficients are equal to unity, as in the case of the powder pattern. Conversely, for samples having a preferential orientation, the corresponding texture coefficient is equal to *N* while the other coefficients are equal to zero.

3. Theory

An ideal ALD process should provide a single monolayer of precursor after each successive exposure. However, when precursor molecules from the gas phase impinge on the substrate surface and begin to stick, a complete monolayer may not be formed due to several factors including the steric hindrance of bulky precursors,[36] or the balance between absorption and desorption kinetics

of precursor molecules (which depends on the deposition pressure, substrate temperature, and precursor concentration in the gas phase). For a given precursor and deposition pressure and temperature, the effect of the precursor concentration in the gas phase on the ALD growth of ZnO film can easily be understood. In the case of the ZnO deposition presented here, we maintained sufficient water supply to ensure surface water saturation. The nitrogen bubbling flow through DEZ container was then varied to study the effect of the concentration of DEZ con the growth rate of ZnO films.

Using a simple model based on Langmuir isotherm adsorption and desorption curves,[37] the growth rate of ZnO at a constant temperature can be theoretically calculated. Be θ(t) the fraction of the surface covered at the time t, the variation of this quantity is simply the difference between the adsorption and desorption rates, expressed as follows:

$$\frac{d\theta(t)}{dt} = k_a[DEZ](1-\theta(t)) - k_d\theta(t) \qquad \text{Eq (2)}$$

where k_a, k_d and $[DEZ]$ refer to the rate constants for the adsorption and desorption processes, and the gas phase concentration of the molecular species (in this case is zinc precursor, DEZ), respectively. This equation can be easily solved, giving the expression of the fraction of surface covered (with the boundary condition ($\theta(t=0)=0$):

$$\theta(t) = \frac{k_a[DEZ]}{k_a[DEZ]+k_d}\left[1-\exp\left(-\left(k_a[DEZ]+k_d\right)t\right)\right] \qquad \text{Eq (3)}$$

In the case of SALD, the deposition is usually carried out at low temperatures and under atmospheric pressure. It can therefore be classed as a high-pressure process. As a first

approximation, we assumed that the desorption rate is small compared to the adsorption rate during the precursor exposure time. Hence, Eq (3) can be rewritten as:

$$\theta(t) = 1 - \exp\left(-k_a \left[DEZ\right] t\right) \qquad \text{Eq (4)}$$

We assume that the GPC is proportional to the fraction of surface coverage θ after each precursor exposure, which is associated with the exposure time, also called residence time t_{res}, calculated from the substrate velocity. Therefore, the dependence of GPC on precursor exposure can be simply expressed as follows:

$$GPC\left(\left[DEZ\right], t_{res}\right) = K_1\left[1 - \exp\left(-k_a \left[DEZ\right] t_{res}\right)\right] \qquad \text{Eq (5)}$$

with K_1 is a constant corresponding to the static growth rate, GPC_0, when using a sufficiently long exposure.

A typical 3D scheme of a SALD injection head is shown in Figure 1a. The head, which is placed at a short distance from the moving substrate, delivers the reactive precursors onto the substrate surface to reproduce ALD cycles, i.e. DEZ/ N_2/ H_2O/ N_2 and so on. If the substrate is immobile and placed close enough to the injection head, Comsol Multiphysics simulation shows that the reactants can be adequately separated from mixing, as shown by gas velocity and precursor concentration profile in Figure 1b and Figure 1c, respectively, and by previous reports.[38] In the close-proximity SALD approach, the precursor exposure depends on several parameters including substrate velocity (*v*), the distance between two adjacent exhaust channels next to the precursor outlets (noted d_{DEZ} or d_{H_2O} as shown in Figure 1c), the concentration of precursor in the gas phase ($\left[DEZ\right]$ or $\left[H_2O\right]$), the gas flow through each channel, as well as the distance between the injection head and the substrate (d_{gap}).

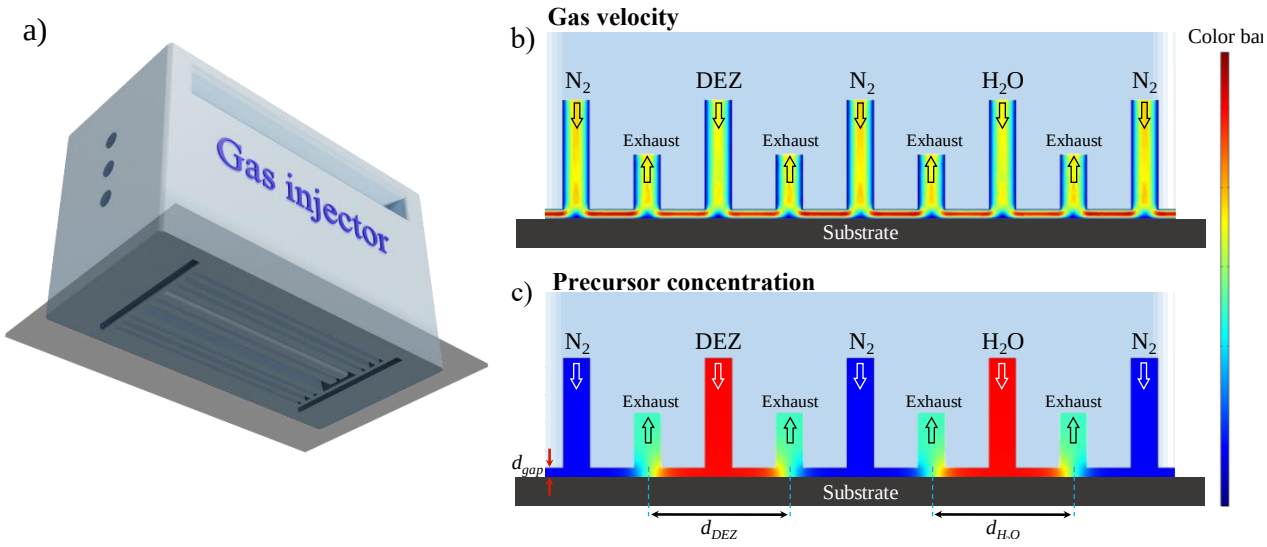

Figure 1: a) 3D scheme of the close-proximity SALD injection head used in this work, represented along with a glass substrate placed underneath the injection head (the typical dimensions of the head are 30×40×50 mm^3), b) gas velocity and c) precursor concentration in such an injector, obtained by Comsol Multiphysics simulation in the case of an immobile substrate. The color bar schematically represents values of velocity and precursor concentration, where the hotter color corresponds to higher values. d_{DEZ}, d_{H_2O} *and* d_{gap} *represent the distances between two adjacent exhaust channels next to the precursor outlets, and the distance between the injection head and the substrate surface, respectively.*

As a first approximation, at a given $[DEZ]$, when the substrate moves at a speed v (cm/s), every point on the substrate will be exposed to DEZ-containing gas during a so-called residence time, $t_{res} = d_{DEZ} / v$, where d_{DEZ} is the distance between two adjacent exhaust channels, as shown in Figure 1c (d_{DEZ} = 2.5 mm in the design shown in Figure 1a). Therefore, GPC versus substrate velocity (v) can be expressed as follows:

$$GPC\left([DEZ], v\right) = K_1\left[1 - \exp\left(-\frac{k_a [DEZ] d_{DEZ}}{v}\right)\right] \qquad \text{Eq (6)}$$

In practice, the precursor concentration in the gas phase, $[DEZ]$, is not easily accessible but it is assumed to be proportional to the nitrogen bubbling flow through DEZ, denoted f_{DEZ}. Therefore, Eq (6) can be rewritten as:

$$GPC\left(f_{DEZ}, v\right) = K_1\left[1 - \exp\left(-\frac{K_2 f_{DEZ} d_{DEZ}}{v}\right)\right] \quad \text{Eq (7)}$$

With K_2 is a constant proportional to the rate constant for the adsorption reaction. This simple equation can be used to study the effect of the substrate velocity or DEZ bubbling flow on the ZnO growth while keeping the other parameters constant. We will see later that the DEZ delivered to the substrate surface is significantly affected by the substrate velocity, leading to a spatial redistribution of the precursor along the substrate surface. The gas molecules at the substrate surface are indeed entrained by the movement of the latter. This effect will be discussed in the next part with simulation and experimental results.

4. Results and discussion

Effect of precursor concentration

As mentioned previously, ALD precursors being usually expensive, an excess injection of precursors to the substrate surface is not desirable. It may also lead to unexpected effects such as precursor condensation or etching, as schematically represented in Figure 2a. The condensation effect is more favorable at high deposition pressure and low-temperature,[37] which is indeed the case of AP-SALD.

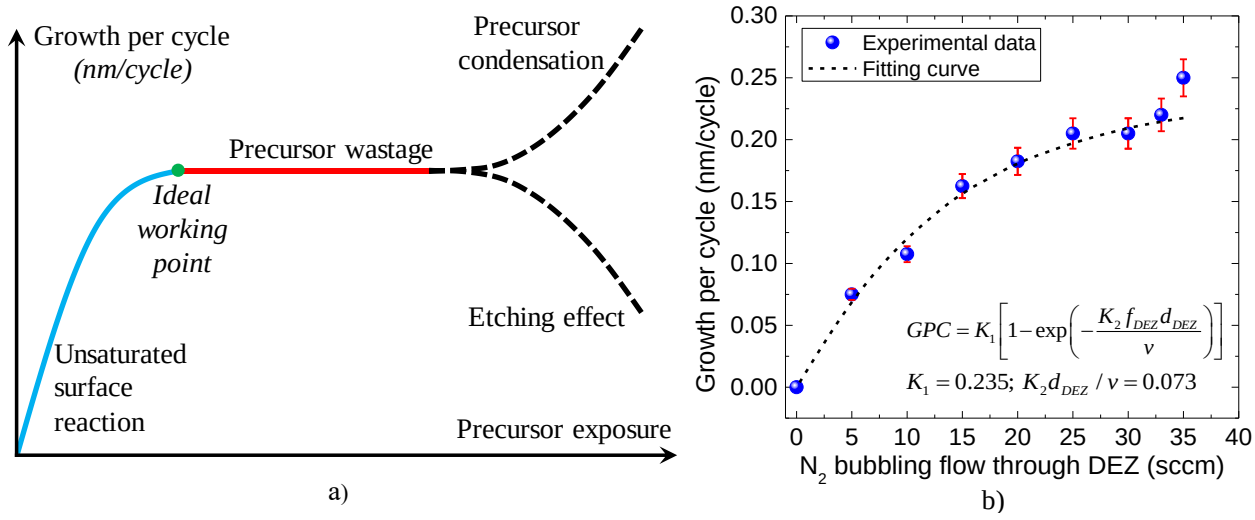

Figure 2: a) a schematic representation of growth per cycle (GPC) versus exposure time, b) Experimental GPC as a function of N_2 bubbling flow through DEZ (sccm). The fit using the simple Langmuir adsorption kinetics model (Eq (7)) is shown by the dashed line for N_2 bubbling flow through DEZ in the range of [0 sccm, 33 sccm]. The substrate velocity, substrate temperature, and injector/substrate gap were fixed at 5 cm/s, 200 °C, and 180 µm, respectively.

Figure 2b shows the experimental data of GPC as a function of f_{DEZ} and the fitting curve using the simple Langmuir adsorption kinetics model presented in Eq (7). In this experiment, the substrate temperature (200 °C), the injector/substrate gap (180 µm), the substrate velocity (5 cm/s), or the N_2 purging flow (150 sccm) was maintained constant and only f_{DEZ} varies. The first fitting parameter K_1 represents the growth rate at the saturating state of the substrate surface, while $K_2 d_{DEZ} / v$ represents a constant depending on the volatility, the adsorption coefficient of $[DEZ]$ and the substrate velocity. The fit results in a growth rate value at the saturating state of the substrate surface of 0.235 nm/cycle, which is comparable to the values found in the literature.[39] The fitting quality is good for low f_{DEZ} values. However, for higher values (f_{DEZ} > 30 sccm), the growth rate becomes faster and cannot be appropriately fitted using the simple model anymore. This might stem from precursor condensation for high f_{DEZ} values. It could also originate from the use of a constant

N_2 purging flow (150 sccm) which is no longer sufficient to remove the excess of DEZ (given the increasing flow of gas through the DEZ channels).

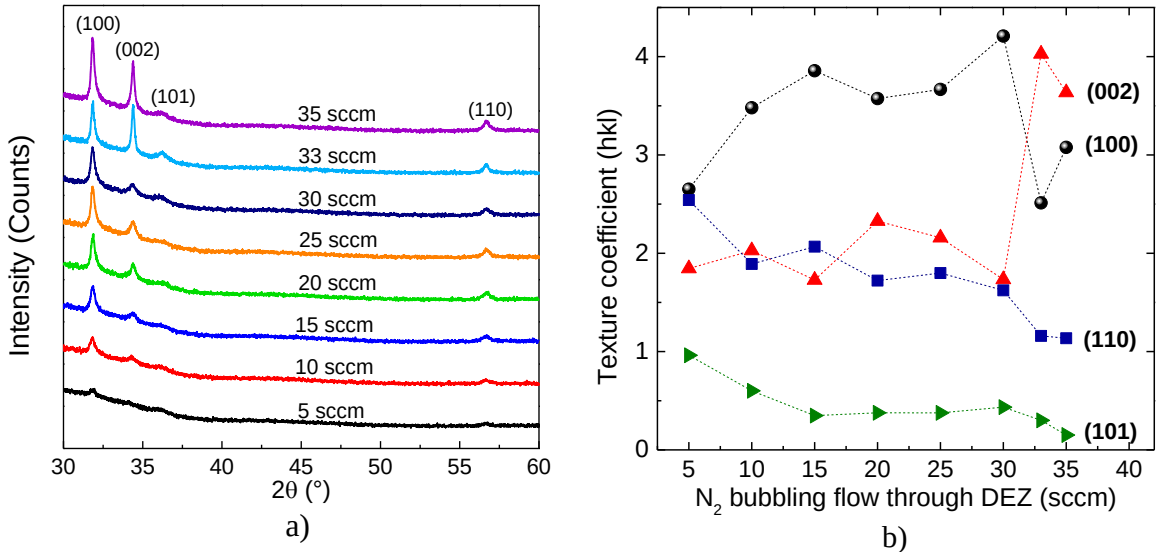

Figure 3: a) X-ray diffraction patterns and b) texture coefficients of ZnO films deposited with different N_2 bubbling flows through DEZ, f_{DEZ}.

The structural properties of the deposited ZnO films with varying precursor concentration were investigated using X-ray diffraction (XRD). Figure 3a shows an increase of the XRD peak intensities of ZnO films versus f_{DEZ}, which is mainly due to the thickness effect. We remark that the samples deposited with small f_{DEZ} values ([10 sccm, 30 sccm]) exhibit similar crystalline nanostructure with (100) reflection as the dominant peak. The texture coefficients corresponding to (110) and (002) reflection peaks are rather close to each other, while the value for the (100) peak is almost twice higher, as shown in Figure 3b. In the cases of f_{DEZ} > 30 sccm, the (002) reflection peak appears more intense compared to the (100) peak, which can also be visualized by an abrupt variation in the texture coefficient. In summary, the precursor concentration in the gas phase, which is related to f_{DEZ} in our case, has a significant impact not only on the film growth rate but also on the nanostructure of the deposited films. Thus, while it has been shown that close-proximity SALD

can be used in CVD mode,[38,40] care must be taken to ensure that the properties of the deposited films are still acceptable for the targeted applications. The ALD condition can thus be achieved by placing the f_{DEZ} value in an appropriate range ([25 sccm, 30 sccm]) to reach the ALD saturation condition while avoiding any precursor condensation.

Effect of substrate velocity on GPC and film properties

Figure 4a shows a 2D Comsol Multiphysics simulation of the DEZ concentration profile at the corresponding injection channel for different values of substrate velocity, i.e. from 0 *cm/s* to 16 *cm/s*. In the case of an immobile substrate, the DEZ concentration profile is symmetric and centered between the two DEZ exhaust channels adjacent to the DEZ channel. When the substrate is moving beneath the gas injector (to the right in this illustration), the precursor molecules are entrained by the moving substrate, creating an asymmetric concentration profile, as observed in Figure 4a.

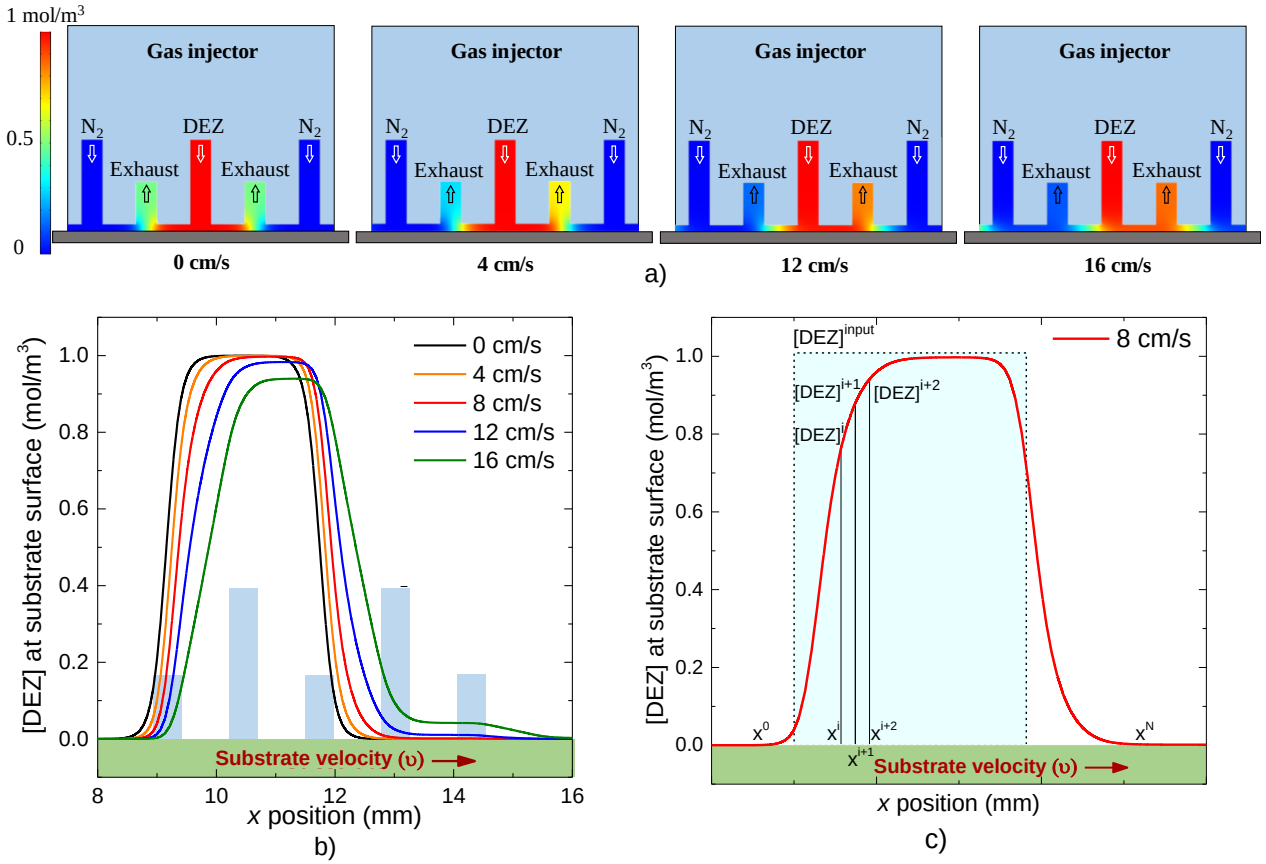

Figure 4: a) DEZ 2D concentration profile at its injection channel for different values of substrate velocity, b) the corresponding DEZ concentration profiles projected at the substrate surface level. In this case, the substrate temperature and the gap between the substrate and the injection head were fixed at 200 °C and 180 µm, respectively, c) schematic illustration of the variation of [DEZ] as a function of position for a substrate velocity of 8 cm/s, as implemented in the proposed model. The data shown here were simulated with Comsol Multiphysics.

As a consequence, the simple relationship between the precursor exposure and the substrate velocity previously shown Eq (6) is no longer appropriate to describe the dependence of the GPC versus the substrate velocity and therefore needs a better approach. Although the precursor concentration in the gas phase is not constant in the vertical direction, the fraction of precursor molecules, that efficiently participate in ALD half-reactions, concerns only the first layers in contact with the substrate. Figure 4b shows this fraction for various substrate velocities. As the substrate

velocity increases, both an asymmetry and a decrease in DEZ concentration are observed. This can be attributed to two main reasons: i) the gas-entraining effect caused by the moving substrate, and ii) the presence of two adjacent exhaust channels located next to the DEZ outlet. Although the high velocity of the substrate could facilitate the mixture of DEZ and H_2O in the gas phase, thus enhancing a CVD contribution to the film growth, our simulations show that this is not the case (see part 3 of the Supporting Information for details).

In an ideal case, the substrate surface would be exposed to a constant concentration of DEZ, namely $[DEZ]^{input}$ as shown in Figure 4c, during a constant exposure time that is simply equal to the ratio of the distance between two adjacent exhaust channels, d_{DEZ}, to the substrate velocity, v. In such a case, the precursor exposure to the substrate surface would be calculated as follows:

$$Ex = \frac{[DEZ]^{input} \cdot d_{DEZ}}{v} \qquad \text{Eq (8)}$$

Where $[DEZ]^{input} \cdot d_{DEZ}$ represents the area of the ideal rectangle shown in Figure 4c. However, the simulation shows that the precursor concentration profiles are not simply constant but quite complex and shifted to the direction of substrate motion. In Figure 4c, we suggest a more meticulous estimation of the effective exposure of DEZ to the substrate surface by discretizing the $[DEZ]$ profiles into N small segments indicated by coordinates $x^0, x^1 \ldots x^N$. If N is large enough, the precursor concentration in each segment $\left[x^i, x^{i+1}\right]$ can be considered constant and the exposure of the precursor to this portion of the substrate would indeed be equal to $[DEZ]^i(x) \cdot dx$. Therefore, we define an effective exposure, $Ex^{effective}$, which can be calculated as follows:

$$Ex^{effective} = \frac{\left(\int_{x_0}^{x_N} [DEZ](x)dx \right)}{v} \qquad \text{Eq (9)}$$

where $A_{[DEZ]} = \int_{x_0}^{x_N} [DEZ](x)dx$ represents the area under the $[DEZ]$ profile.

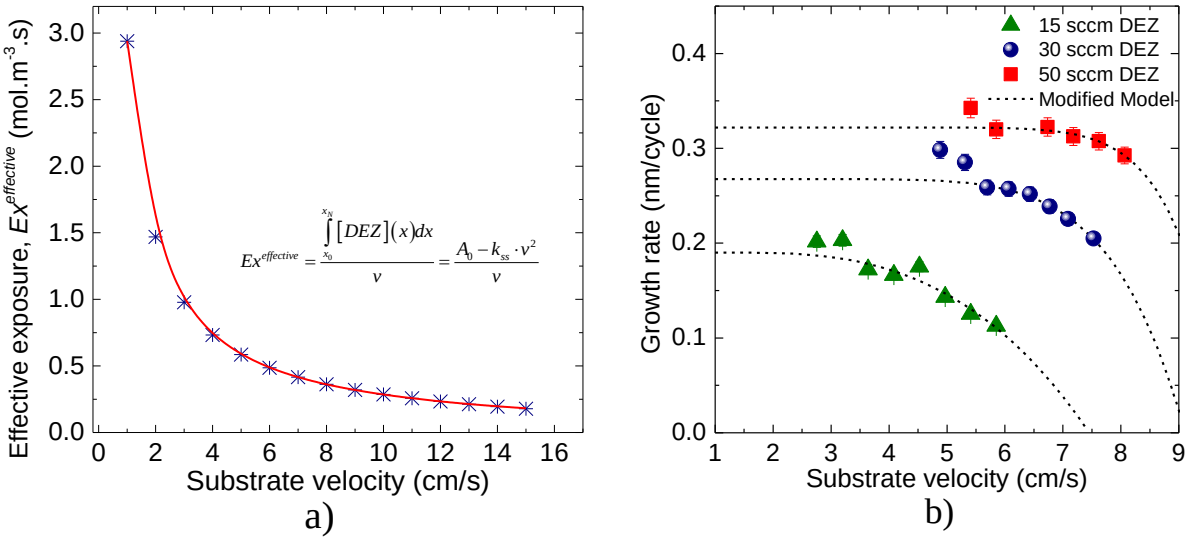

Figure 5: a) Simulation result of the effective exposure ($Ex^{effective}$) versus substrate velocity and the fit using a simple second-order polynomial regression; b) experimental values of the growth per cycle of ZnO films as a function of the substrate velocity, and DEZ bubbling flows, and the associated fits using Eq (10)

Figure 5a illustrates the effective exposure as a function of the substrate velocity (data obtained from Comsol Multiphysics simulation). Interestingly, the behavior of $A_{[DEZ]}$ versus substrate velocity, v, can be appropriately fitted by using a second-order polynomial regression without the linear term as a first approximation to reduce the number of fitting parameters to only A_0 and k_{ss}: $A_{[DEZ]} = A_0 - k_{ss} \cdot v^2$. Here, A_0 corresponds to the symmetric $[DEZ]$ distribution under the precursor channel when the substrate is immobile (v = 0 cm/s). k_{ss} is a constant depending on many parameters including the DEZ concentration in the gas phase, the viscosity of the mixed gas,

as well as the substrate temperature. According to this simulation result, the exposure shown in the Eq (6) is not simply inversely proportional to the substrate velocity, but there exists an effective exposure, as shown in Figure 5a. Hence, a new physical approach towards $GPC(v)$ can be calculated as follows:

$$GPC(v) = K_1\left\{1-\exp\left[-k_a\left(\frac{A_0}{v}-k_{ss}v\right)\right]\right\} \qquad \text{Eq (10)}$$

The right side of Eq (10) can be simplified by setting $X = k_a A_0$ and $Y = k_a k_{ss}$. Figure 5b shows the experimental data and corresponding fitting curves using Eq (10) for the GPC of ZnO films deposited at different $[DEZ]$ values as a function of substrate velocity, v. Our model properly fits the data of the high and intermediate substrate velocities for various DEZ bubbling flow rates (15, 30 and 50 sccm). Conversely, it can be observed that the growth rates deviate from the theoretical model at low substrate velocities, which correspond to the longer exposure time. As discussed in Figure 2, an extra injection of precursors to the substrate surface can create condensation if the subsequent purging step is not sufficiently long. This fact was not taken into account in our simple model, yielding an underestimation of the growth rate at low substrate velocities. The same argument could also explain the increase of the static growth rate, K_1, obtained at higher values of f_{DEZ} (30 or 50 sccm compared to 15 sccm). Indeed, the N_2 purging flow should be adapted for each value of f_{DEZ} and substrate velocity. However, in this work, it was maintained constant at 150 sccm to keep the gas flow balance at all the outlets of the injection head. Consequently, this value may not be sufficient to purge the excess physisorbed precursor molecules in the case of high $[DEZ]$. Concerning the fitting parameters, while K_1 is associated with the static growth rate, X and Y do not have a direct physical meaning. On the contrary, the

ratio between Y and X is equal to the ratio between A_0 and k_{ss}, which can be related to the effective exposure t_{res}^{eff} as follows:

$$Ex^{effective} = \frac{A_0 - k_{ss}v^2}{v} = k_{ss}\left(\frac{v_c^{\,2} - v^2}{v}\right) \qquad \text{Eq (11)}$$

where $v_c = \sqrt{Y/X}$ is a characteristic velocity (cm/s). Intuitively, when the substrate velocity approaches this critical value, the effective exposure would rapidly decrease, which yields a lower growth rate. The summary of the parameters extracted from the fits is shown in Table 1. The static growth rate obtained when using the value of f_{DEZ} equal to 30 sccm is about 0.27 nm/cycle, which is indeed similar to the value obtained in a conventional thermal ALD process at atmospheric pressure.[39]

Table 1: Some critical parameters extracted or calculated from the fits shown in Figure 5b.

f_{DEZ} (sccm)	K_1 (nm/cycle)	v_c (cm/s)	k_{ss} (s^2cm^{-4})
15	0.19	7.46	0.24
30	0.27	9.11	0.41
50	0.32	9.83	0.61

In general, experimental parameters should be optimized to obtain a fast deposition rate, which is indeed a compromise between a high substrate velocity and a long enough residence time. Therefore, according to Eq (7) and Eq (8), high values of k_{ss} and v_c are expected. Since k_{ss} characterizes how easily the DEZ flow can be entrained by the moving substrate, the observed decreasing trend of k_{ss} versus f_{DEZ} indicates that the growth rate of ZnO is less affected by the

substrate velocity if higher DEZ bubbling flow is used. The opposite trend is observed for v_c. A higher value of this characteristic velocity is expected given the fact that a fast substrate velocity can be used while maintaining a constant t_{res}^{eff}. From another point of view, the optimization of the SALD process concerns the improvement of the growth rate with as little as possible precursor consumption. Three pivotal parameters should be taken into account: growth rate GPC (nm/cycle), precursor consumption that is directly proportional to f_{DEZ} (sccm) and deposition time t_{dep} (s), of which the latter is related to the substrate velocity v (cm/s). Let η_{dep} denote a parameter combining these factors, namely process efficiency, and be written as follows:

$$\eta_{dep} = \frac{GPC \cdot v}{f_{DEZ}} \qquad \text{Eq (7)}$$

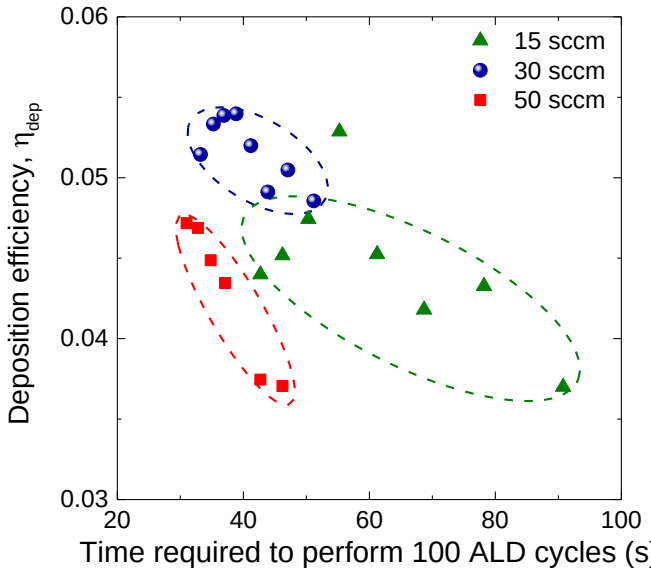

Figure 6: Process efficiency as a function of the time required to perform 100 ALD cycles in the case of ZnO deposition by SALD.

Figure 6 describes the variation of process efficiency η_{dep} as a function of the time required to perform a constant number of cycles (for example 100 cycles in this illustration). It can be

calculated by using the experimental data shown in Figure 5b. A longer deposition time corresponds to a slower substrate velocity and leads to a high precursor consumption, which makes, in general, a low process efficiency. On the other hand, using the low value of f_{DEZ} (15 sccm) can save precursor, however, the disadvantage is a longer deposition time to maintain a constant process efficiency. Remarkably, using a moderate value of f_{DEZ} (30 sccm) yields a significantly higher value of efficiency η_{dep}. This interesting observation provides a guide on how to optimize the SALD deposition process by controlling at the same time the precursor consumption and the deposition time.

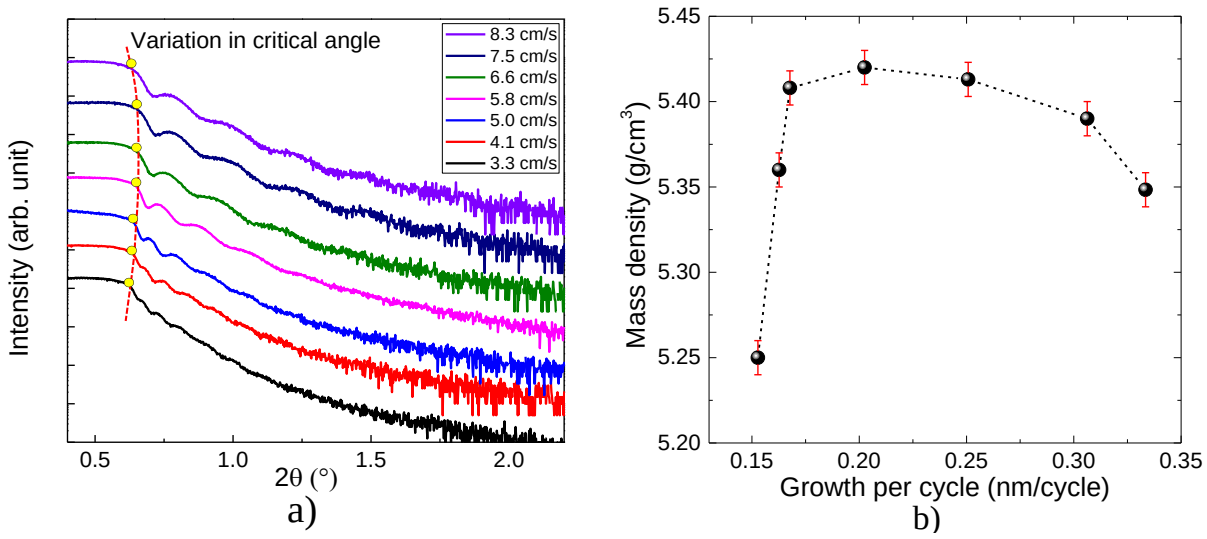

Figure 7:a) XRR patterns of ZnO films deposited at different substrate velocities (substrate temperature: 200 °C). The variation of critical angle indicates the change in the mass density of the deposited film, b) Mass density (g/cm^3) as a function of growth rate (nm/cycle). In this example, ZnO thin films deposited by AP-SALD using an N_2 bubbling flow through DEZ of 25 sccm.

Apart from the growth rate, other important features that have to be considered such as film density. Figure 7a shows the XRR patterns of ZnO films deposited at various substrate velocities in the range of [3.3, 8.3 cm/s], from which two important parameters can be extracted, i.e. film mass density and thickness. This range of substrate velocities generates a variation in film thickness from 27.5 nm to 60 nm, which corresponds to GPC values in between [0.15, 0.33 nm/cyc]. Figure

7b shows the dependence of the mass density of the deposited ZnO films on the growth rate. An optimum range of GPC values corresponding to a maximum mass density of 5.42 g/cm^3 can be appreciated, while the bulk value is expected to be 5.61 g/cm^3. For high GPC values (≥ 0.3 nm/cycle), the lower mass density of the deposited films can be related to excess precursor physisorbed on the substrate surface, making somehow a mixed-CVD-ALD deposition mode rather than pure ALD mode. In the case of slower growth rates (< 0.2 nm/s), corresponding to non-saturating ALD surface reaction, the low mass density values could be related to the film thickness effect. Indeed, ZnO thin films prepared by SALD at 200 °C using diethylzinc result in polycrystalline structure, in which the grain size (and therefore the film density) significantly depends on the film thickness. The dependence of the optical properties of ZnO films deposited by SALD on the substrate velocity is also discussed in part 2 of the Supporting Information.

5. Conclusions

In this work, simulation and experimental studies have been conducted to study the effect of a critical parameter, namely, precursor exposure in the case of a close-proximity spatial atomic layer deposition (SALD) approach. This parameter depends directly on the substrate velocity, the geometric design of the injection head, as well as the carrier gas flow rate. A simple physical model has been developed to study the effect of the substrate velocity and the precursor concentration in the carrier gas ($[DEZ]$) on the growth rate of the deposited ZnO films. Comsol Multiphysics results show that the entrainment of the precursor molecules by the moving substrate induces an asymmetry in $[DEZ]$ profile that affects the obtained growth per cycle (GPC). When studying thoroughly the experimental data based on the effect of $[DEZ]$ and the substrate velocity at constant $[DEZ]$, we found that an excess of physisorbed precursor molecules on the substrate

surface in the case of high $[DEZ]$ can be indirectly observed via the clear variation of the film growth rate when either increasing $[DEZ]$ or decreasing the substrate velocity beyond a certain value. The agreement between experimental observations and the model appears very good. Finally, we have also shown that the mass density of the ZnO deposited film depends closely on the substrate velocity, and that a fast growth rate does not always produce dense films. Indeed, a compromise between the growth rate and the precursor consumption should be considered to obtain both a high film density and a good process efficiency, of which the latter is proposed for the first time to quantify such analysis in SALD. The proposed simple and original approach can pave the way to better understand thin film growth using any SALD system, since it provides a comprehensive guide on optimizing growth rate, film density, and precursor consumption. This is indeed crucial when using SALD for large-scale coating applications.

Acknowledgments

This work was funded by the Agence Nationale de Recherche (ANR, France) via the programs ANR-16-CE05-0021 (DESPATCH), ANR-18-CE09-0041 (Meaning), ANR-18-CE09-0036 (Panassé) and ANR-17-CE05-0034 (Oxygen). This work was supported by the European Joint Doctorate FunMAT program (H2020-MSCA-ITN-2014, Project ID 641640). This project was also supported by the French National Research Agency in the framework of the "Investissements d'avenir" program (ANR-15-IDEX-02) through the project Eco-SESA. This work was also performed within the framework of the Centre of Excellence of Multifunctional Architectured Materials "CEMAM" no. AN-10-LABX-44-01. This work was as well supported by Région Auvergne Rhône-Alpes through the project Pack Ambition Recherche 2018 Eternité. The Carnot Energies du Futur is acknowledged through the project FREE. David Muñoz-Rojas

acknowledges funding through the Marie Curie Actions (FP7/2007–2013, Grant 631111). The authors would like to warmly thank L. Rapenne for her technical assistance, and Dr. César Masse de la Huerta and Dr. Hao Van Bui for fruitful discussions.

References

[1] S.M. George, Atomic Layer Deposition: An Overview, Chemical Reviews. 110 (2010) 111–131. https://doi.org/10.1021/cr900056b.

[2] H. Van Bui, F. Grillo, J.R. van Ommen, Atomic and molecular layer deposition: off the beaten track, Chemical Communications. 53 (2017) 45–71. https://doi.org/10.1039/C6CC05568K.

[3] V. Cremers, R.L. Puurunen, J. Dendooven, Conformality in atomic layer deposition: Current status overview of analysis and modelling, Applied Physics Reviews. 6 (2019) 021302. https://doi.org/10.1063/1.5060967.

[4] R.W. Johnson, A. Hultqvist, S.F. Bent, A brief review of atomic layer deposition: from fundamentals to applications, Materials Today. 17 (2014) 236–246. https://doi.org/10.1016/j.mattod.2014.04.026.

[5] L. Mai, D. Zanders, E. Subaşı, E. Ciftyurek, C. Hoppe, D. Rogalla, W. Gilbert, T. de los Arcos, K. Schierbaum, G. Grundmeier, C. Bock, A. Devi, Low-Temperature Plasma-Enhanced Atomic Layer Deposition of Tin(IV) Oxide from a Functionalized Alkyl Precursor: Fabrication and Evaluation of SnO_2 -Based Thin-Film Transistor Devices, ACS Appl. Mater. Interfaces. 11 (2019) 3169–3180. https://doi.org/10.1021/acsami.8b16443.

[6] O. Graniel, M. Weber, S. Balme, P. Miele, M. Bechelany, Atomic layer deposition for biosensing applications, Biosensors and Bioelectronics. 122 (2018) 147–159. https://doi.org/10.1016/j.bios.2018.09.038.

[7] J.-S. Park, H. Chae, H.K. Chung, S.I. Lee, Thin film encapsulation for flexible AM-OLED: a review, Semicond. Sci. Technol. 26 (2011) 034001. https://doi.org/10.1088/0268-1242/26/3/034001.

[8] T. Maindron, T. Jullien, A. André, Defect analysis in low temperature atomic layer deposited Al_2O_3 and physical vapor deposited SiO barrier films and combination of both to achieve high quality moisture barriers, Journal of Vacuum Science & Technology A: Vacuum, Surfaces, and Films. 34 (2016) 031513. https://doi.org/10.1116/1.4947289.

[9] A.K. Singh, K. Adstedt, B. Brown, P.M. Singh, S. Graham, Development of ALD Coatings for Harsh Environment Applications, ACS Appl. Mater. Interfaces. 11 (2019) 7498–7509. https://doi.org/10.1021/acsami.8b11557.

[10] A. Khan, V.H. Nguyen, D. Muñoz-Rojas, S. Aghazadehchors, C. Jiménez, N.D. Nguyen, D. Bellet, Stability Enhancement of Silver Nanowire Networks with Conformal ZnO Coatings Deposited by Atmospheric Pressure Spatial Atomic Layer Deposition, ACS Applied Materials & Interfaces. 10 (2018) 19208–19217. https://doi.org/10.1021/acsami.8b03079.

[11] V.H. Nguyen, J. Resende, D.T. Papanastasiou, N. Fontanals, C. Jiménez, D. Muñoz-Rojas, D. Bellet, Low-cost fabrication of flexible transparent electrodes based on Al doped ZnO and silver nanowire nanocomposites: impact of the network density, Nanoscale. 11 (2019) 12097–12107. https://doi.org/10.1039/C9NR02664A.

[12] R. Liu, Y. Lin, L.-Y. Chou, S.W. Sheehan, W. He, F. Zhang, H.J.M. Hou, D. Wang, Water Splitting by Tungsten Oxide Prepared by Atomic Layer Deposition and Decorated with an Oxygen-Evolving Catalyst, Angewandte Chemie International Edition. 50 (2011) 499–502. https://doi.org/10.1002/anie.201004801.

[13] X. Meng, X.-Q. Yang, X. Sun, Emerging Applications of Atomic Layer Deposition for Lithium-Ion Battery Studies, Advanced Materials. 24 (2012) 3589–3615. https://doi.org/10.1002/adma.201200397.

[14] H.V. Bui, F. Grillo, S. Sharath Kulkarni, R. Bevaart, N.V. Thang, B. van der Linden, J. A. Moulijn, M. Makkee, M. T. Kreutzer, J.R. van Ommen, Low-temperature atomic layer deposition delivers more active and stable Pt-based catalysts, Nanoscale. 9 (2017) 10802–10810. https://doi.org/10.1039/C7NR02984E.

[15] M.-W. Kim, K. Kim, T.Y. Ohm, H. Yoon, B. Joshi, E. Samuel, M.T. Swihart, S.K. Choi, H. Park, S.S. Yoon, Electrosprayed BiVO4 nanopillars coated with atomic-layer-deposited ZnO/TiO2 as highly efficient photoanodes for solar water splitting, Chemical Engineering Journal. 333 (2018) 721–729. https://doi.org/10.1016/j.cej.2017.09.130.

[16] F. Grillo, H. Van Bui, D. La Zara, A.A.I. Aarnink, A.Y. Kovalgin, P. Kooyman, M.T. Kreutzer, J.R. van Ommen, From Single Atoms to Nanoparticles: Autocatalysis and Metal Aggregation in Atomic Layer Deposition of Pt on TiO_2 Nanopowder, Small. 14 (2018) 1800765. https://doi.org/10.1002/smll.201800765.

[17] M. Liu, F. Xue, X. Wang, W. Fu, Y. Wang, Y. Lu, N. Li, Conformal deposition of atomic TiO2 layer on chalcogenide nanorod with excellent activity and durability towards solar H2 generation, Chemical Engineering Journal. 341 (2018) 335–343. https://doi.org/10.1016/j.cej.2018.02.031.

[18] W.-Z. Fang, Y.-Q. Tang, C. Ban, Q. Kang, R. Qiao, W.-Q. Tao, Atomic layer deposition in porous electrodes: A pore-scale modeling study, Chemical Engineering Journal. 378 (2019) 122099. https://doi.org/10.1016/j.cej.2019.122099.

[19] D. Muñoz-Rojas, T. Maindron, A. Esteve, F. Piallat, J.C.S. Kools, J.-M. Decams, Speeding up the unique assets of atomic layer deposition, Materials Today Chemistry. 12 (2019) 96–120. https://doi.org/10.1016/j.mtchem.2018.11.013.

[20] A.S. Yersak, K. Sharma, J.M. Wallas, A.A. Dameron, X. Li, Y. Yang, K.E. Hurst, C. Ban, R.C. Tenent, S.M. George, Spatial atomic layer deposition for coating flexible porous Li-ion battery electrodes, Journal of Vacuum Science & Technology A: Vacuum, Surfaces, and Films. 36 (2018) 01A123. https://doi.org/10.1116/1.5006670.

[21] A. Illiberi, F. Roozeboom, P. Poodt, Spatial atomic layer deposition of zinc oxide thin films., ACS Applied Materials & Interfaces. 4 (2012) 268–72. https://doi.org/10.1021/am2013097.

[22] A. Illiberi, R. Scherpenborg, Y. Wu, F. Roozeboom, P. Poodt, Spatial Atmospheric Atomic Layer Deposition of AlxZn1-xO., ACS Applied Materials & Interfaces. 5 (2013) 13124–8. https://doi.org/10.1021/am404137e.

[23] D. Muñoz-Rojas, V.H. Nguyen, C. Masse de la Huerta, S. Aghazadehchors, C. Jiménez, D. Bellet, Spatial Atomic Layer Deposition (SALD), an emerging tool for energy materials. Application to new-generation photovoltaic devices and transparent conductive materials, Comptes Rendus Physique. 18 (2017) 391–400. https://doi.org/10.1016/j.crhy.2017.09.004.

[24] K.P. Musselman, C.F. Uzoma, M.S. Miller, Nanomanufacturing: High-Throughput, Cost-Effective Deposition of Atomic Scale Thin Films via Atmospheric Pressure Spatial Atomic Layer Deposition, Chem. Mater. 28 (2016) 8443–8452. https://doi.org/10.1021/acs.chemmater.6b03077.

[25] G.N. Parsons, S.M. George, M. Knez, Progress and future directions for atomic layer deposition and ALD-based chemistry, MRS Bull. 36 (2011) 865–871. https://doi.org/10.1557/mrs.2011.238.

[26] D.H. Levy, D. Freeman, S.F. Nelson, P.J. Cowdery-Corvan, L.M. Irving, Stable ZnO thin film transistors by fast open air atomic layer deposition, Applied Physics Letters. 92 (2008) 192101. https://doi.org/10.1063/1.2924768.

[27] R.L.Z. Hoye, D. Muñoz-Rojas, S.F. Nelson, A. Illiberi, P. Poodt, F. Roozeboom, J.L. MacManus-Driscoll, Research Update: Atmospheric pressure spatial atomic layer deposition of ZnO thin films: Reactors, doping, and devices, APL Materials. 3 (2015) 040701. https://doi.org/10.1063/1.4916525.

[28] S.D. Elliott, Atomic-scale simulation of ALD chemistry, Semicond. Sci. Technol. 27 (2012) 074008. https://doi.org/10.1088/0268-1242/27/7/074008.

[29] R.L. Puurunen, Surface chemistry of atomic layer deposition: A case study for the trimethylaluminum/water process, Journal of Applied Physics. 97 (2005) 121301. https://doi.org/10.1063/1.1940727.

[30] F. Grillo, M.T. Kreutzer, J.R. van Ommen, Modeling the precursor utilization in atomic layer deposition on nanostructured materials in fluidized bed reactors, Chemical Engineering Journal. 268 (2015) 384–398. https://doi.org/10.1016/j.cej.2015.01.067.

[31] Y. Xie, L. Ma, D. Pan, C. Yuan, Mechanistic modeling of atomic layer deposition of alumina process with detailed surface chemical kinetics, Chemical Engineering Journal. 259 (2015) 213–220. https://doi.org/10.1016/j.cej.2014.07.105.

[32] P. Poodt, J. van Lieshout, A. Illiberi, R. Knaapen, F. Roozeboom, A. van Asten, On the kinetics of spatial atomic layer deposition, Journal of Vacuum Science & Technology A: Vacuum, Surfaces, and Films. 31 (2013) 01A108. https://doi.org/10.1116/1.4756692.

[33] Z. Deng, W. He, C. Duan, R. Chen, B. Shan, Mechanistic modeling study on process optimization and precursor utilization with atmospheric spatial atomic layer deposition, Journal of Vacuum Science & Technology A: Vacuum, Surfaces, and Films. 34 (2016) 01A108. https://doi.org/10.1116/1.4932564.

[34] V.H. Nguyen, D. Bellet, B. Masenelli, D. Muñoz-Rojas, Increasing the Electron Mobility of ZnO-Based Transparent Conductive Films Deposited by Open-Air Methods for Enhanced Sensing Performance, ACS Applied Nano Materials. 1 (2018) 6922–6931. https://doi.org/10.1021/acsanm.8b01745.

[35] S. Aghazadehchors, V.H. Nguyen, D. Muñoz-Rojas, C. Jiménez, L. Rapenne, N.D. Nguyen, D. Bellet, Versatility of bilayer metal oxide coatings on silver nanowire networks for enhanced stability with minimal transparency loss, Nanoscale. 11 (2019) 19969–19979. https://doi.org/10.1039/C9NR05658K.

[36] S. Kim, S. Lee, S.-Y. Ham, D.-H. Ko, S. Shin, Z. Jin, Y.-S. Min, A kinetic study of ZnO atomic layer deposition: Effects of surface hydroxyl concentration and steric hindrance, Applied Surface Science. 469 (2019) 804–810. https://doi.org/10.1016/j.apsusc.2018.11.064.

[37] C. Tien, Introduction to Adsorption: Basics, Analysis, and Applications, Elsevier, 2018.

[38] C. Masse de la Huerta, V.H. Nguyen, J.-M. Dedulle, D. Bellet, C. Jiménez, D. Muñoz-Rojas, Influence of the Geometric Parameters on the Deposition Mode in Spatial Atomic Layer Deposition: A Novel Approach to Area-Selective Deposition, Coatings. 9 (2019) 5. https://doi.org/10.3390/coatings9010005.

[39] M.B.M. Mousa, C.J. Oldham, J.S. Jur, G.N. Parsons, Effect of temperature and gas velocity on growth per cycle during Al2O3 and ZnO atomic layer deposition at atmospheric pressure, Journal of Vacuum Science & Technology A: Vacuum, Surfaces, and Films. 30 (2012) 01A155. https://doi.org/10.1116/1.3670961.

[40] K.P. Musselman, D. Muñoz-Rojas, R.L.Z. Hoye, H. Sun, S.-L. Sahonta, E. Croft, M.L. Böhm, C. Ducati, J.L. MacManus-Driscoll, Rapid open-air deposition of uniform, nanoscale, functional coatings on nanorod arrays, Nanoscale Horizons. 2 (2017) 110–117. https://doi.org/10.1039/C6NH00197A.